PHYSICAL REVIEW D **88,** 031103(R) (2013)

Signature-based search for delayed photons in exclusive photon plus missing transverse energy events from $p\bar{p}$ collisions with $\sqrt{s} = 1.96$ TeV

T. Aaltonen,[21] S. Amerio,[40a] D. Amidei,[32] A. Anastassov,[15,y] A. Annovi,[17] J. Antos,[12] G. Apollinari,[15] J. A. Appel,[15] T. Arisawa,[53] A. Artikov,[13] J. Asaadi,[48] W. Ashmanskas,[15] B. Auerbach,[2] A. Aurisano,[48] F. Azfar,[39] W. Badgett,[15] T. Bae,[25] A. Barbaro-Galtieri,[26] V. E. Barnes,[44] B. A. Barnett,[23] P. Barria,[42c,42a] P. Bartos,[12] M. Bauce,[40b,40a] F. Bedeschi,[42a] S. Behari,[15] G. Bellettini,[42b,42a] J. Bellinger,[55] D. Benjamin,[14] A. Beretvas,[15] A. Bhatti,[46] K. R. Bland,[5] B. Blumenfeld,[23] A. Bocci,[14] A. Bodek,[45] D. Bortoletto,[44] J. Boudreau,[43] A. Boveia,[11] L. Brigliadori,[6b,6a] C. Bromberg,[33] E. Brucken,[21] J. Budagov,[13] H. S. Budd,[45] K. Burkett,[15] G. Busetto,[40b,40a] P. Bussey,[19] P. Butti,[42b,42a] A. Buzatu,[19] A. Calamba,[10] S. Camarda,[4] M. Campanelli,[28] F. Canelli,[11,15,ee] B. Carls,[22] D. Carlsmith,[55] R. Carosi,[42a] S. Carrillo,[16,n] B. Casal,[9,l] M. Casarsa,[49a] A. Castro,[6b,6a] P. Catastini,[20] D. Cauz,[49a] V. Cavaliere,[22] M. Cavalli-Sforza,[4] A. Cerri,[26,f] L. Cerrito,[28,t] Y. C. Chen,[1] M. Chertok,[7] G. Chiarelli,[42a] G. Chlachidze,[15] K. Cho,[25] D. Chokheli,[13] M. A. Ciocci,[42c,42a] A. Clark,[18] C. Clarke,[54] M. E. Convery,[15] J. Conway,[7] M. Corbo,[15] M. Cordelli,[17] C. A. Cox,[7] D. J. Cox,[7] M. Cremonesi,[42a] D. Cruz,[48] J. Cuevas,[9,aa] R. Culbertson,[15] N. d'Ascenzo,[15,x] M. Datta,[15,gg] P. De Barbaro,[45] L. Demortier,[46] M. Deninno,[6a] M. d'Errico,[40b,40a] F. Devoto,[21] A. Di Canto,[42b,42a] B. Di Ruzza,[15,r] J. R. Dittmann,[5] M. D'Onofrio,[27] S. Donati,[42b,42a] M. Dorigo,[49b,49a] A. Driutti,[49a] K. Ebina,[53] R. Edgar,[32] A. Elagin,[48] R. Erbacher,[7] S. Errede,[22] B. Esham,[22] R. Eusebi,[48] S. Farrington,[39] J. P. Fernández Ramos,[29] R. Field,[16] G. Flanagan,[15,v] R. Forrest,[7] M. Franklin,[20] J. C. Freeman,[15] H. Frisch,[11] Y. Funakoshi,[53] A. F. Garfinkel,[44] P. Garosi,[42c,42a] H. Gerberich,[22] E. Gerchtein,[15] S. Giagu,[47a] V. Giakoumopoulou,[3] K. Gibson,[43] C. M. Ginsburg,[15] N. Giokaris,[3] P. Giromini,[17] G. Giurgiu,[23] V. Glagolev,[13] D. Glenzinski,[15] M. Gold,[35] D. Goldin,[48] A. Golossanov,[15] G. Gomez,[9] G. Gomez-Ceballos,[30] M. Goncharov,[30] O. González López,[29] I. Gorelov,[35] A. T. Goshaw,[14] K. Goulianos,[46] E. Gramellini,[6a] S. Grinstein,[4] C. Grosso-Pilcher,[11] R. C. Group,[52,15] J. Guimaraes da Costa,[20] S. R. Hahn,[15] J. Y. Han,[45] F. Happacher,[17] K. Hara,[50] M. Hare,[51] R. F. Harr,[54] T. Harrington-Taber,[15,o] K. Hatakeyama,[5] C. Hays,[39] J. Heinrich,[41] M. Herndon,[55] A. Hocker,[15] Z. Hong,[48] W. Hopkins,[15,g] S. Hou,[1] R. E. Hughes,[36] U. Husemann,[56] M. Hussein,[33,h] J. Huston,[33] G. Introzzi,[42e,42a] M. Iori,[47b,47a] A. Ivanov,[7,q] E. James,[15] D. Jang,[10] B. Jayatilaka,[15] E. J. Jeon,[25] S. Jindariani,[15] M. Jones,[44] K. K. Joo,[25] S. Y. Jun,[10] T. R. Junk,[15] M. Kambeitz,[24] T. Kamon,[25,48] P. E. Karchin,[54] A. Kasmi,[5] Y. Kato,[38,p] W. Ketchum,[11,hh] J. Keung,[41] B. Kilminster,[15,ee] D. H. Kim,[25] H. S. Kim,[25] J. E. Kim,[25] M. J. Kim,[17] S. B. Kim,[25] S. H. Kim,[50] Y. J. Kim,[25] Y. K. Kim,[11] N. Kimura,[53] M. Kirby,[15] K. Knoepfel,[15] K. Kondo,[53,a] D. J. Kong,[25] J. Konigsberg,[16] A. V. Kotwal,[14] M. Kreps,[24] J. Kroll,[41] M. Kruse,[14] T. Kuhr,[24] M. Kurata,[50] A. T. Laasanen,[44] S. Lammel,[15] M. Lancaster,[28] K. Lannon,[36,z] G. Latino,[42c,42a] H. S. Lee,[25] J. S. Lee,[25] S. Leo,[42a] S. Leone,[42a] J. D. Lewis,[15] A. Limosani,[14,u] E. Lipeles,[41] A. Lister,[18,b] H. Liu,[52] Q. Liu,[44] T. Liu,[15] S. Lockwitz,[56] A. Loginov,[56] A. Lucà,[17] D. Lucchesi,[40b,40a] J. Lueck,[24] P. Lujan,[26] P. Lukens,[15] G. Lungu,[46] J. Lys,[26] R. Lysak,[12,e] R. Madrak,[15] P. Maestro,[42c,42a] S. Malik,[46] G. Manca,[27,c] A. Manousakis-Katsikakis,[3] F. Margaroli,[47a] P. Marino,[42d,42a] M. Martínez,[4] K. Matera,[22] M. E. Mattson,[54] A. Mazzacane,[15] P. Mazzanti,[6a] R. McNulty,[27,k] A. Mehta,[27] P. Mehtala,[21] C. Mesropian,[46] T. Miao,[15] D. Mietlicki,[32] A. Mitra,[1] H. Miyake,[50] S. Moed,[15] N. Moggi,[6a] C. S. Moon,[15,bb] R. Moore,[15,ff] M. J. Morello,[42d,42a] A. Mukherjee,[15] Th. Muller,[24] P. Murat,[15] M. Mussini,[6b,6a] J. Nachtman,[15,o] Y. Nagai,[50] J. Naganoma,[53] I. Nakano,[37] A. Napier,[51] J. Nett,[48] C. Neu,[52] T. Nigmanov,[43] L. Nodulman,[2] S. Y. Noh,[25] O. Norniella,[22] L. Oakes,[39] S. H. Oh,[14] Y. D. Oh,[25] I. Oksuzian,[52] T. Okusawa,[38] R. Orava,[21] L. Ortolan,[4] C. Pagliarone,[49a] E. Palencia,[9,f] P. Palni,[35] V. Papadimitriou,[15] W. Parker,[55] G. Pauletta,[49c,49a] M. Paulini,[10] C. Paus,[30] T. J. Phillips,[14] G. Piacentino,[42a] E. Pianori,[41] J. Pilot,[36] K. Pitts,[22] C. Plager,[8] L. Pondrom,[55] S. Poprocki,[15,g] K. Potamianos,[26] A. Pranko,[26] F. Prokoshin,[13,cc] F. Ptohos,[17,i] G. Punzi,[42b,42a] N. Ranjan,[44] I. Redondo Fernández,[29] P. Renton,[39] M. Rescigno,[47a] F. Rimondi,[6a,a] L. Ristori,[42a,15] A. Robson,[19] T. Rodriguez,[41] S. Rolli,[51,j] M. Ronzani,[42b,42a] R. Roser,[15] J. L. Rosner,[11] F. Ruffini,[42c,42a] A. Ruiz,[9] J. Russ,[10] V. Rusu,[15] W. K. Sakumoto,[45] Y. Sakurai,[53] L. Santi,[49c,49a] K. Sato,[50] V. Saveliev,[15,x] A. Savoy-Navarro,[15,bb] P. Schlabach,[15] E. E. Schmidt,[15] T. Schwarz,[32] L. Scodellaro,[9] F. Scuri,[42a] S. Seidel,[35] Y. Seiya,[38] A. Semenov,[13] F. Sforza,[42b,42a] S. Z. Shalhout,[7] T. Shears,[27] P. F. Shepard,[43] M. Shimojima,[50,w] M. Shochet,[11] I. Shreyber-Tecker,[34] A. Simonenko,[13] P. Sinervo,[31] K. Sliwa,[51] J. R. Smith,[7] F. D. Snider,[15] H. Song,[43] V. Sorin,[4] M. Stancari,[15] R. St. Denis,[19] B. Stelzer,[31] O. Stelzer-Chilton,[31] D. Stentz,[15,y] J. Strologas,[35] Y. Sudo,[50] A. Sukhanov,[15] I. Suslov,[13] K. Takemasa,[50] Y. Takeuchi,[50] J. Tang,[11] M. Tecchio,[32] P. K. Teng,[1] J. Thom,[15,g] E. Thomson,[41] V. Thukral,[48] D. Toback,[48] S. Tokar,[12] K. Tollefson,[33] T. Tomura,[50] D. Tonelli,[15,f] S. Torre,[17] D. Torretta,[15] P. Totaro,[40a] M. Trovato,[42d,42a] F. Ukegawa,[50] S. Uozumi,[25] F. Vázquez,[16,n] G. Velev,[15] C. Vellidis,[15] C. Vernieri,[42d,42a] M. Vidal,[44] R. Vilar,[9] J. Vizán,[9,dd] M. Vogel,[35] G. Volpi,[17] P. Wagner,[41] R. Wallny,[8] S. M. Wang,[1] A. Warburton,[31] D. Waters,[28] W. C. Wester III,[15] D. Whiteson,[41,d] A. B. Wicklund,[2] S. Wilbur,[11] H. H. Williams,[41] J. S. Wilson,[32] P. Wilson,[15] B. L. Winer,[36] P. Wittich,[15,g]

S. Wolbers,[15] H. Wolfe,[36] T. Wright,[32] X. Wu,[18] Z. Wu,[5] K. Yamamoto,[38] D. Yamato,[38] T. Yang,[15] U. K. Yang,[11,s] Y. C. Yang,[25] W.-M. Yao,[26] G. P. Yeh,[15] K. Yi,[15,o] J. Yoh,[15] K. Yorita,[53] T. Yoshida,[38,m] G. B. Yu,[14] I. Yu,[25] A. M. Zanetti,[49a] Y. Zeng,[14] C. Zhou,[14] and S. Zucchelli[6b,6a]

(CDF Collaboration)

[1]*Institute of Physics, Academia Sinica, Taipei, Taiwan 11529, Republic of China*
[2]*Argonne National Laboratory, Argonne, Illinois 60439, USA*
[3]*University of Athens, 157 71 Athens, Greece*
[4]*Institut de Fisica d'Altes Energies, ICREA, Universitat Autonoma de Barcelona, E-08193 Bellaterra (Barcelona), Spain*
[5]*Baylor University, Waco, Texas 76798, USA*
[6a]*Istituto Nazionale di Fisica Nucleare Bologna, I-40127 Bologna, Italy*
[6b]*University of Bologna, I-40127 Bologna, Italy*
[7]*University of California, Davis, California 95616, USA*
[8]*University of California, Los Angeles, California 90024, USA*
[9]*Instituto de Fisica de Cantabria, CSIC-University of Cantabria, 39005 Santander, Spain*
[10]*Carnegie Mellon University, Pittsburgh, Pennsylvania 15213, USA*
[11]*Enrico Fermi Institute, University of Chicago, Chicago, Illinois 60637, USA*
[12]*Comenius University, 842 48 Bratislava, Slovakia; Institute of Experimental Physics, 040 01 Kosice, Slovakia*
[13]*Joint Institute for Nuclear Research, RU-141980 Dubna, Russia*
[14]*Duke University, Durham, North Carolina 27708, USA*
[15]*Fermi National Accelerator Laboratory, Batavia, Illinois 60510, USA*
[16]*University of Florida, Gainesville, Florida 32611, USA*
[17]*Laboratori Nazionali di Frascati, Istituto Nazionale di Fisica Nucleare, I-00044 Frascati, Italy*
[18]*University of Geneva, CH-1211 Geneva 4, Switzerland*
[19]*Glasgow University, Glasgow G12 8QQ, United Kingdom*
[20]*Harvard University, Cambridge, Massachusetts 02138, USA*
[21]*Division of High Energy Physics, Department of Physics, University of Helsinki and Helsinki Institute of Physics, FIN-00014 Helsinki, Finland*
[22]*University of Illinois, Urbana, Illinois 61801, USA*
[23]*The Johns Hopkins University, Baltimore, Maryland 21218, USA*
[24]*Institut für Experimentelle Kernphysik, Karlsruhe Institute of Technology, D-76131 Karlsruhe, Germany*
[25]*Center for High Energy Physics: Kyungpook National University, Daegu 702-701, Korea; Seoul National University, Seoul 151-742, Korea; Sungkyunkwan University, Suwon 440-746, Korea; Korea Institute of Science and Technology Information, Daejeon 305-806, Korea; Chonnam National University, Gwangju 500-757, Korea; Chonbuk National University, Jeonju 561-756, Korea; Ewha Womans University, Seoul 120-750, Korea*
[26]*Ernest Orlando Lawrence Berkeley National Laboratory, Berkeley, California 94720, USA*
[27]*University of Liverpool, Liverpool L69 7ZE, United Kingdom*
[28]*University College London, London WC1E 6BT, United Kingdom*
[29]*Centro de Investigaciones Energeticas Medioambientales y Tecnologicas, E-28040 Madrid, Spain*
[30]*Massachusetts Institute of Technology, Cambridge, Massachusetts 02139, USA*
[31]*Institute of Particle Physics: McGill University, Montréal, Québec H3A 2T8, Canada; Simon Fraser University, Burnaby, British Columbia V5A 1S6, Canada; University of Toronto, Toronto, Ontario M5S 1A7, Canada; and TRIUMF, Vancouver, British Columbia V6T 2A3, Canada*
[32]*University of Michigan, Ann Arbor, Michigan 48109, USA*
[33]*Michigan State University, East Lansing, Michigan 48824, USA*
[34]*Institution for Theoretical and Experimental Physics, ITEP, Moscow 117259, Russia*
[35]*University of New Mexico, Albuquerque, New Mexico 87131, USA*
[36]*The Ohio State University, Columbus, Ohio 43210, USA*
[37]*Okayama University, Okayama 700-8530, Japan*
[38]*Osaka City University, Osaka 588, Japan*
[39]*University of Oxford, Oxford OX1 3RH, United Kingdom*
[40a]*Istituto Nazionale di Fisica Nucleare, Sezione di Padova-Trento, I-35131 Padova, Italy*
[40b]*University of Padova, I-35131 Padova, Italy*
[41]*University of Pennsylvania, Philadelphia, Pennsylvania 19104, USA*
[42a]*Istituto Nazionale di Fisica Nucleare Pisa, I-56127 Pisa, Italy*
[42b]*University of Pisa, I-56127 Pisa, Italy*
[42c]*University of Siena, I-56127 Pisa, Italy*
[42d]*Scuola Normale Superiore, I-56127 Pisa, Italy*
[42e]*INFN Pavia and University of Pavia, I-27100 Pavia, Italy*

[43]University of Pittsburgh, Pittsburgh, Pennsylvania 15260, USA
[44]Purdue University, West Lafayette, Indiana 47907, USA
[45]University of Rochester, Rochester, New York 14627, USA
[46]The Rockefeller University, New York, New York 10065, USA
[47a]Istituto Nazionale di Fisica Nucleare, Sezione di Roma 1, I-00185 Roma, Italy
[47b]Sapienza Università di Roma, I-00185 Roma, Italy
[48]Mitchell Institute for Fundamental Physics and Astronomy, Texas A&M University, College Station, Texas 77843, USA
[49a]Istituto Nazionale di Fisica Nucleare Trieste/Udine, I-34127 Trieste, Italy
[49b]University of Trieste, I-34127 Trieste, Italy
[49c]University of Udine, I-33100 Udine, Italy
[50]University of Tsukuba, Tsukuba, Ibaraki 305, Japan
[51]Tufts University, Medford, Massachusetts 02155, USA
[52]University of Virginia, Charlottesville, Virginia 22906, USA
[53]Waseda University, Tokyo 169, Japan
[54]Wayne State University, Detroit, Michigan 48201, USA
[55]University of Wisconsin, Madison, Wisconsin 53706, USA
[56]Yale University, New Haven, Connecticut 06520, USA
(Received 2 July 2013; published 23 August 2013)

We present the first signature-based search for delayed photons using an exclusive photon plus missing transverse energy final state. Events are reconstructed in a data sample from the CDF II detector corresponding to 6.3 fb^{-1} of integrated luminosity from $\sqrt{s} = 1.96$ TeV proton-antiproton collisions. Candidate events are selected if they contain a photon with an arrival time in the detector larger than expected from a promptly produced photon. The mean number of events from standard model sources predicted by the data-driven background model based on the photon timing distribution is 286 ± 24. A total of 322 events are observed. A p value of 12% is obtained, showing consistency of the data with standard model predictions.

DOI: 10.1103/PhysRevD.88.031103 PACS numbers: 14.80.Nb, 12.60.Jv, 13.85.Qk

[a]Deceased.
[b]Visitor from University of British Columbia, Vancouver, BC V6T 1Z1, Canada.
[c]Visitor from Istituto Nazionale di Fisica Nucleare, Sezione di Cagliari, 09042 Monserrato (Cagliari), Italy.
[d]Visitor from University of California Irvine, Irvine, CA 92697, USA.
[e]Visitor from Institute of Physics, Academy of Sciences of the Czech Republic, 182~21, Czech Republic.
[f]Visitor from CERN, CH-1211 Geneva, Switzerland.
[g]Visitor from Cornell University, Ithaca, NY 14853, USA.
[h]Visitor from The University of Jordan, Amman 11942, Jordan.
[i]Visitor from University of Cyprus, Nicosia CY-1678, Cyprus.
[j]Visitor from Office of Science, U.S. Department of Energy, Washington, DC 20585, USA.
[k]Visitor from University College Dublin, Dublin 4, Ireland.
[l]Visitor from ETH, 8092 Zürich, Switzerland.
[m]Visitor from University of Fukui, Fukui City, Fukui Prefecture, Japan 910-0017.
[n]Visitor from Universidad Iberoamericana, Lomas de Santa Fe, México, C.P. 01219, Distrito Federal.
[o]Visitor from University of Iowa, Iowa City, IA 52242, USA.
[p]Visitor from Kinki University, Higashi-Osaka City, Japan 577-8502.
[q]Visitor from Kansas State University, Manhattan, KS 66506, USA.
[r]Visitor from Brookhaven National Laboratory, Upton, NY 11973, USA.
[s]Visitor from University of Manchester, Manchester M13 9PL, United Kingdom.
[t]Visitor from Queen Mary, University of London, London, E1 4NS, United Kingdom.
[u]Visitor from University of Melbourne, Victoria 3010, Australia.
[v]Visitor from Muons, Inc., Batavia, IL 60510, USA.
[w]Visitor from Nagasaki Institute of Applied Science, Nagasaki 851-0193, Japan.
[x]Visitor from National Research Nuclear University, Moscow 115409, Russia.
[y]Visitor from Northwestern University, Evanston, IL 60208, USA.
[z]Visitor from University of Notre Dame, Notre Dame, IN 46556, USA.
[aa]Visitor from Universidad de Oviedo, E-33007 Oviedo, Spain.
[bb]Visitor from CNRS-IN2P3, Paris, F-75205 France.
[cc]Visitor from Universidad Tecnica Federico Santa Maria, 110v Valparaiso, Chile.
[dd]Visitor from Universite catholique de Louvain, 1348 Louvain-La-Neuve, Belgium.
[ee]Visitor from University of Zürich, 8006 Zürich, Switzerland.
[ff]Visitor from Massachusetts General Hospital and Harvard Medical School, Boston, MA 02114 USA.
[gg]Visitor from Hampton University, Hampton, VA 23668, USA.
[hh]Visitor from Los Alamos National Laboratory, Los Alamos, NM 87544, USA.

The unknown nature of possible particles or interactions beyond the standard model (SM) motivates search strategies at particle collider experiments that do not rely on features of specific phenomenological models, but rather seek generic deviations from the SM expectations [1]. We report a signature-based search in exclusive photon and missing transverse energy ($\not\!\!E_T$) [2] events from proton-antiproton ($p\bar{p}$) collisions at $\sqrt{s} = 1.96$ GeV where candidate events are selected based on photons that arrive late in the detector relative to the time expected from prompt production (*delayed* photon). This would be the signature of a heavy, neutral, long-lived particle that traverses part of the detector and then decays to a photon and a neutral, noninteracting particle that would appear in the detector as $\not\!\!E_T$ [3,4]. Such particles would exist, for example, in gauge-mediated supersymmetry-breaking scenarios (e.g., $\tilde{\chi}_1^0 \to \gamma\tilde{G}$, where $\tilde{\chi}_1^0$ is the lightest neutralino and $\tilde{G}$ is the gravitino) [5]. Searches that focus on particular models at collider experiments, where supersymmetric particles appear at the end of a decay chain, found no evidence for these particles [6,7]. We focus on the exclusive $\gamma + \not\!\!E_T$ final state with delayed photons. Since the sensitivity to such scenarios can vary significantly as a function of the model parameters (e.g., production mechanism as well as the mass and lifetime of the heavy, non-SM particle) [3,4], we conduct a signature-based search and present the results without any optimization or limit interpretation with respect to a particular model.

This paper summarizes the first such search and uses data from 6.3 fb^{-1} of integrated luminosity collected with the CDF II detector at the Fermilab Tevatron [8]. An important variable in this search is the difference between the observed arrival time of a photon in the detector and the time predicted for photons promptly produced in the primary $p\bar{p}$ interaction. This difference in time, Δt, is used to distinguish signal candidate events from both SM-collision and noncollision background sources. For photons produced in decays of heavy, long-lived particles, the distribution in Δt would be shifted towards positive values [3]. A full estimation of the backgrounds to the photon and missing energy final state is performed in a data-driven manner and compared to data to determine whether any significant excess of events exists.

Detailed descriptions of the CDF II detector can be found elsewhere [9]. The detector subsystems relevant to this analysis are briefly mentioned here. The event kinematic properties and detector geometry are described in a cylindrical coordinate system [2]. The detector is composed of a silicon microstrip tracking system (''silicon vertex detector''), a tracking drift chamber, a calorimeter detector, and a muon detector. The silicon vertex detector provides a high-precision position measurement of charged-particle trajectories [10], while the drift chamber provides accurate momentum measurements and allows the reconstruction of each charged particle's production time [11]. The combination of these measurements provides accurate reconstruction of the position ($\vec{x}_{\rm i}$) and time ($t_{\rm i}$) of the primary $p\bar{p}$ interaction. The $p\bar{p}$ luminous region is approximately described by a Gaussian distribution centered at $z_{\rm i} = 0$ with an rms spread of 28 cm and mean time of $t_{\rm i} = 0$ with an rms spread of 1.28 ns. The $p\bar{p}$ interactions are reconstructed using an algorithm that combines well measured tracks to form a candidate vertex [6]. Vertex candidates must consist of at least three high-quality tracks that intersect each other within 1.5 cm along the z axis and within 1.5 ns in time, with $\Sigma p_T \geq 5$ GeV and $|z| < 60$ cm, where $\sum p_T$ is the scalar sum of the transverse momenta of the corresponding charged particles. The reconstructed vertices use the average z and t of the tracks and have a spatial resolution of 0.24 cm in z and a time resolution of 0.22 ns.

The calorimeter has a pointing-tower geometry and is composed of separate electromagnetic and hadronic compartments that are used to identify photons, electrons, jets, and muons, as well as measure $\not\!\!E_T$ in the event. The measurement of the arrival time ($t_{\rm f}$) of photons (and electrons) in the electromagnetic calorimeter is done using a fixed-threshold discriminator and a time-to-digital converter system [12] which is connected to each electromagnetic tower and has a resolution of 0.60 ns. The measurement of the arrival position ($\vec{x}_{\rm f}$) is measured by the shower-maximum detector in the electromagnetic calorimeter (radius = 184 cm) and has a resolution of 0.2 cm [13].

The CDF experiment uses a multitrigger online data acquisition system. This analysis uses events selected with a trigger that requires a photon candidate having at least 25 GeV of E_T, in addition to a requirement of at least 25 GeV of $\not\!\!E_T$ in the event. By also allowing candidate events from one or more additional photon triggers [6], we achieve approximately 100% efficiency for events passing the final selection requirements [6].

In the offline analysis, photon candidates are required to meet standard photon identification requirements with a minor modification as described in Ref. [6], to retain efficiency for photons that do not come directly from the beam line. For reasons described below, the offline photon E_T and event $\not\!\!E_T$ values are calculated with respect to the center of the detector (E_T^0 and $\not\!\!E_T^0$) rather than the selected primary vertex. Backgrounds from noncollision sources (cosmic rays and beam-halo sources) are rejected using standard criteria [6,14] along with new requirements [15] that render the beam-halo background negligible.

Collision backgrounds in the exclusive $\gamma + \not\!\!E_T$ data sample result from processes of γ + jets production, where unreconstructed jets mimic $\not\!\!E_T$; $Z\gamma \to \nu\nu\gamma$ production; $W \to l\nu$ production, where the lepton or an extraneous jet is misidentified as a photon; and $W(\gamma) \to l\nu\gamma$ production, where the lepton is not identified. Raising the E_T^0 and $\not\!\!E_T^0$ thresholds to 45 GeV and requiring the exclusive $\gamma + \not\!\!E_T$ final state rejects most of these backgrounds; any event

with a reconstructed track with $p_T > 10$ GeV/c and rapidity magnitude $|\eta| < 1.6$ [2] is excluded from the analysis. Similarly, events are rejected if they contain an additional energy cluster, reconstructed with the JETCLU algorithm [16] with a $\Delta R = 0.4$ cone, with $E_T > 15$ GeV.

We calculate Δt for each photon candidate using

$$\Delta t = (t_{\rm f} - t_{\rm i}) - {\rm TOF}, \quad (1)$$

where ${\rm TOF} = (|\vec{x}_{\rm f} - \vec{x}_{\rm i}|)/c$ is the expected time of flight of a prompt photon from the selected $p\bar{p}$ interaction vertex to the location of the associated energy deposit in the calorimeter. For a promptly produced photon, $\Delta t = 0$ ns in a hypothetical detector with perfect timing resolution. The signal region for this analysis is defined as $2 < \Delta t < 7$ ns to remove most promptly produced photons at small values of Δt and cosmic-ray events at large times but retain heavy, long-lived particles that would have decayed before leaving the detector [3]. If multiple vertices are reconstructed in the event, the vertex with the highest $\sum p_T$ is selected as the primary vertex.

The background contributions from noncollision and collision sources are estimated from data. The noncollision backgrounds are dominated by cosmic-ray sources [6] that are distributed uniformly in time. They are modeled using a data-driven background estimate using events in the region of $20 < \Delta t < 80$ ns and an extrapolation into the signal region. The collision backgrounds can be divided into two classes of events. The first class includes events in which the photon is correctly associated with its production vertex and are readily reduced by the final timing requirement. The second class includes events in which the primary vertex is incorrectly selected as the production vertex of the photon.

The dominant collision background in the signal region comes from prompt SM-photon production events in which the photon is associated with the wrong primary vertex. A wrong vertex assignment can occur either because the $p\bar{p}$ interaction that produced the photon was not reconstructed or because an additional $p\bar{p}$ interaction produced another vertex that was mistakenly associated with the photon. Although it can only be done on a statistical basis, each collision-background event can be classified as a *right-vertex* or a *wrong-vertex* event. While the probability of an event being a wrong-vertex type is dependent on the number of extra collisions in the event or the instantaneous luminosity, the fraction of each type can be measured in data.

Monte Carlo simulations of all the expected SM background processes were performed to aid in their study and rejection. The simulated samples are $W \to e\nu_e$, $W \to \mu\nu_\mu$, $W \to \tau\nu_\tau$, γ + jet, $Z\gamma \to \nu\nu\gamma$ (all produced by the PYTHIA event generator [17], which adds initial- and final-state radiation), and $W(\gamma) \to l\nu\gamma$ (produced by the BAUR event generator [18]). The detector response in all simulation samples, including multiple collisions in the event, is modeled by a GEANT-based detector simulation [19] and allows each event to be classified as a right-vertex or wrong-vertex event. This analysis also uses a control sample of exclusive $e + \not\!\!E_T$ collision events [20] because the final state differs from exclusive $\gamma + \not\!\!E_T$ final state only in the charged-particle track associated with the electron. In such events, the electron track is removed from the event reconstruction to emulate exclusive $\gamma + \not\!\!E_T$ events and then used *a posteriori* to determine whether the emulated photon is correctly associated with its production vertex.

The Δt distributions for right-vertex and wrong-vertex events, $\Delta t^{\rm R}$ and $\Delta t^{\rm W}$, respectively, are both well modeled by Gaussian distributions after all selection requirements. The distribution describing right-vertex events has a mean timing of $\langle \Delta t^{\rm R} \rangle = 0.0 \pm 0.05$ ns and rms spread of 0.65 ± 0.05 ns [12], due to the contributions of the vertex-reconstruction algorithm and the calorimeter-timing resolutions. The distribution describing wrong-vertex collision events has an rms spread of 2.0 ± 0.1 ns [12]. Its mean depends on the associated SM processes and cannot be assumed *a priori*. Since the collision-background timing distribution is described by the sum of the right-vertex and wrong-vertex event distributions, the collective collision background is modeled by the sum of two Gaussian distributions. Five of the six parameters describing these two Gaussian distributions are directly determined from the $\gamma + \not\!\!E_T$ candidate-event data sample since the region $-2 \lesssim \Delta t \lesssim 2$ ns is dominated by right-vertex events and the region with large negative times $-7 \lesssim \Delta t \lesssim -2$ ns is dominated by wrong-vertex events. An independent measurement, for example $\langle \Delta t^{\rm W} \rangle$, is still needed to correctly model the collision backgrounds.

The crucial element of this analysis is that the wrong-vertex timing distribution is well described by a Gaussian whose mean can be measured in a data-driven manner. To motivate the additional selection requirements, Eq. (1) can be rewritten in a form that illustrates the sources of non-Gaussian tails and nonzero mean times for wrong-vertex events. Since $t_{\rm f}$ equals $t_{\rm i}^{\rm R} + {\rm TOF}^{\rm R}$ for SM background events, in the absence of detector effects, the measured Δt when a wrong vertex is selected can be approximated as

$$\Delta t^{\rm W} = (t_{\rm i}^{\rm R} - t_{\rm i}^{\rm W}) + ({\rm TOF}^{\rm R} - {\rm TOF}^{\rm W}), \quad (2)$$

where we continue the use of the superscripts R and W for the variables. The first term in the right-hand side of Eq. (2) has a mean value of zero with an rms spread of $\sqrt{2} \times 1.28$ ns $= 1.8$ ns resulting from the luminous-region parameters. Additional variation due to the measurement of the arrival time brings the full rms spread to 2.0 ns [12]. The rms spread of the background-dependent second term is typically smaller than 0.4 ns, but three effects introduce process-specific non-Gaussian tails and $\mathcal{O}(0.1)$ ns biases on the mean.

The first source of wrong-vertex timing bias is a threshold effect that affects events with the photon E_T near the

analysis threshold of 45 GeV. Use of the wrong vertex position in photon reconstruction biases the measured value of the photon transverse energy ($E_T^{\rm m}$) with respect to its true value ($E_T^{\rm t}$) for geometric reasons. If E_T is defined as $E_T = E\sin\theta$, where θ is the photon-momentum polar angle defined with respect to the primary vertex, selection of the wrong vertex results in misreconstruction of the photon E_T. If the selection of the wrong vertex results in a shorter path length from the collision to the calorimeter, then the E_T is overestimated and the second term in Eq. (2) is positive ($\mathrm{TOF^R} > \mathrm{TOF^W}$). Events with photon $E_T^{\rm t} < 45$ GeV and $E_T^{\rm m} > 45$ GeV contribute to the sample with an average $\Delta t^{\rm W}$ value biased towards larger times. Similarly, an event with a photon with $E_T^{\rm t} > 45$ GeV but $E_T^{\rm m} < 45$ GeV is removed from the sample because of the negative bias of $\Delta t^{\rm W}$. In this case, $\Delta t^{\rm W}$ is biased toward negative times. Thus, an E_T threshold biases the $\Delta t^{\rm W}$ distribution towards positive $\Delta t^{\rm W}$ values. In order to minimize this bias, the detector center ($z = 0.0$) is used in computing E_T (and $\not\!\!E_T$ for consistency).

The second source of wrong-vertex timing bias arises because the primary vertex is required to have $|z| < 60$ cm. Photons in events originating from collisions which occurred at $|z| > 60$ cm would necessarily have the wrong vertex used to compute Δt. This case induces a positive bias in the timing of the second term in the right-hand side of Eq. (2) because the path length from the selected vertex to the calorimeter is biased to shorter values than the true path length. To suppress this source of background, the analysis vetoes events with a vertex with $|z| > 60$ cm using a vertex-identification algorithm that has high efficiency for collisions at large $|z|$ [21]. This requirement is 95% efficient for events with a correctly reconstructed primary vertex satisfying $|z| < 60$ cm.

The last significant source of wrong-vertex timing bias is from $W \to e\nu$ events identified as $\gamma + \not\!\!E_T$ in a way that biases $\langle \Delta t^{\rm W}\rangle$ towards positive values. In this case, as the electron traverses the tracking system, it loses most of its energy to a high-energy photon via bremsstrahlung. As the trajectory of the low-energy electron is curved away from the final photon direction, the photon candidate passes all the photon-identification criteria. In the case that a wrong vertex is selected, the reconstructed photon candidate timing is biased to a positive value of the second term in the right-hand side of Eq. (2). This occurs because electrons with a longer path length are more likely to generate a photon via bremsstrahlung in the detector, and thus the actual path length traversed is longer on average than that of a prompt photon produced in the collision. To reject events in which the electron track does not point to the photon position in the calorimeter, an extra requirement is imposed on reconstructed tracks that are close to the photon in $\eta - \phi$ space, as measured at the beam line. An event is rejected if any reconstructed track in it has a value of $\sqrt{(\Delta\eta/\sigma_\eta)^2 + (\Delta\phi/\sigma_\phi)^2} < 5.0$, where $\Delta\eta$ and $\Delta\phi$ are the differences between the η and ϕ of the track and that of the photon, respectively, and $\sigma_\eta = 6.3 \times 10^{-3}$ and $\sigma_\phi = 8.1 \times 10^{-2}$ are the detector resolutions in $\Delta\eta$ and $\Delta\phi$, respectively [8]. Studies show that this requirement is approximately 95% efficient for prompt photons and reduces the background rate from this source by about 70%.

After imposing all of these bias-reducing restrictions, the resulting sample contains 5421 $\gamma + \not\!\!E_T$ candidates.

The wrong-vertex events in each MC simulation and $e + \not\!\!E_T$ control sample have a timing distribution that is well modeled by a single Gaussian distribution with an rms spread of 2.0 ± 0.1 ns and a mean that varies among the production mechanisms between 0.0 and 0.8 ns. With mean variations across samples not exceeding half of the measured rms spread, any combination of the Δt distributions for the modeled background processes is found to be well modeled by a single Gaussian distribution with the same rms spread within uncertainties. However, the mean value of $\Delta t^{\rm W}$ for the data must be determined separately.

Since the mean of the wrong-vertex timing events lies in the region dominated by right-vertex events, no fit procedure is sensitive enough to determine $\langle \Delta t^{\rm W}\rangle$ with adequate accuracy. To determine $\langle \Delta t^{\rm W}\rangle$, a sample of events independent of the exclusive $\gamma + \not\!\!E_T$ sample is created. This event sample is identical to the $\gamma + \not\!\!E_T$ sample, except for a requirement that there be no reconstructed vertex, and contains 4924 events. The value of Δt for an event that does not have a reconstructed vertex, denoted Δt^0, is computed assuming an initial time and position of $t_{\rm i} = 0$ and $z_{\rm i} = 0$ in Eq. (1). For geometric reasons, $\langle \Delta t^0\rangle = \langle \Delta t^{\rm W}\rangle$ to a high degree of precision for the entire sample; this is observed in all simulation and control samples as shown in Fig. 1. The largest discrepancy is 0.08 ns and is taken as the systematic uncertainty on the measurement of $\langle \Delta t^{\rm W}\rangle$. The Δt^0 distribution is well described by a single Gaussian with an rms spread of 1.6 ± 0.08 ns and a normalization that is determined from data. Note that the rms spread for Δt^0 is

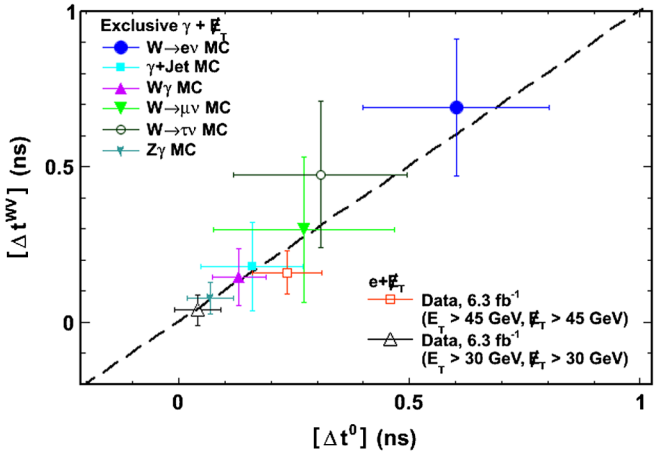

FIG. 1 (color online). A comparison of $\langle \Delta t^{\rm W}\rangle$ and $\langle \Delta t^0\rangle$ in a number of Monte Carlo samples that produce the exclusive $\gamma + \not\!\!E_T$ final state and two exclusive $e + \not\!\!E_T$ data samples.

smaller than the rms spread for Δt^{W} because in Eq. (2) there is variation from not subtracting off the right-vertex information as well as having subtracted off the wrong information. In Δt^0 there is no variation from having added wrong-vertex information.

The data from events both with and without a vertex are combined to estimate the full set of backgrounds. The data outside the signal region are fit to the sum of the two Gaussian distributions and the uniform distribution that describe the complete background model. For the no-vertex sample, a single Gaussian and uniform distribution are used. A likelihood fit is performed over events with a vertex in the bins spanning $-7 < \Delta t < 2$ ns and $20 < \Delta t < 80$ ns and for events without a vertex in the bins spanning $-3.5 < \Delta t^0 < 3.5$ ns and $20 < \Delta t^0 < 80$ ns, which are expected to be dominated by collision and cosmic-ray backgrounds. The likelihood function is defined as a product of Poisson probabilities over the bins of Δt and Δt^0 and Gaussian constraints assigned for each systematic uncertainty.

The best-fit values for the two samples (without and with vertices) are shown in Figs. 2(a) and 2(b). A value of $\langle \Delta t^0 \rangle = \langle \Delta t^{\mathrm{W}} \rangle = 0.20 \pm 0.13$ ns is obtained from the fit. Likewise, in the sample of events with a vertex, 875 ± 66 right-vertex events, 676 ± 84 wrong-vertex events, and 31.9 ± 0.7 events/ns from cosmic rays are obtained. In the signal region, the fit predicts a background of 286 ± 24 events. The contributions include 159 ± 4 cosmic-ray events, 126 ± 24 wrong-vertex events, and 1.0 ± 0.6 right-vertex events. The uncertainty on the background is dominated by the limited number of events in the sample without a reconstructed vertex. The statistical uncertainty on $\langle \Delta t^{\mathrm{W}} \rangle$ produces a 22-event uncertainty on the number of wrong-vertex events in the signal region. The remaining uncertainties are all smaller and are dominated by the systematic uncertainty on the relationship between $\langle \Delta t^{\mathrm{W}} \rangle$ and $\langle \Delta t^0 \rangle$, the uncertainty on the rms spread of $\langle \Delta t^{\mathrm{W}} \rangle$, and the uncertainties on the mean and rms spread for $\langle \Delta t^{\mathrm{R}} \rangle$.

The Δt distribution for the data and backgrounds in the region $-10 < \Delta t < 10$ ns is shown in Fig. 2(c). The

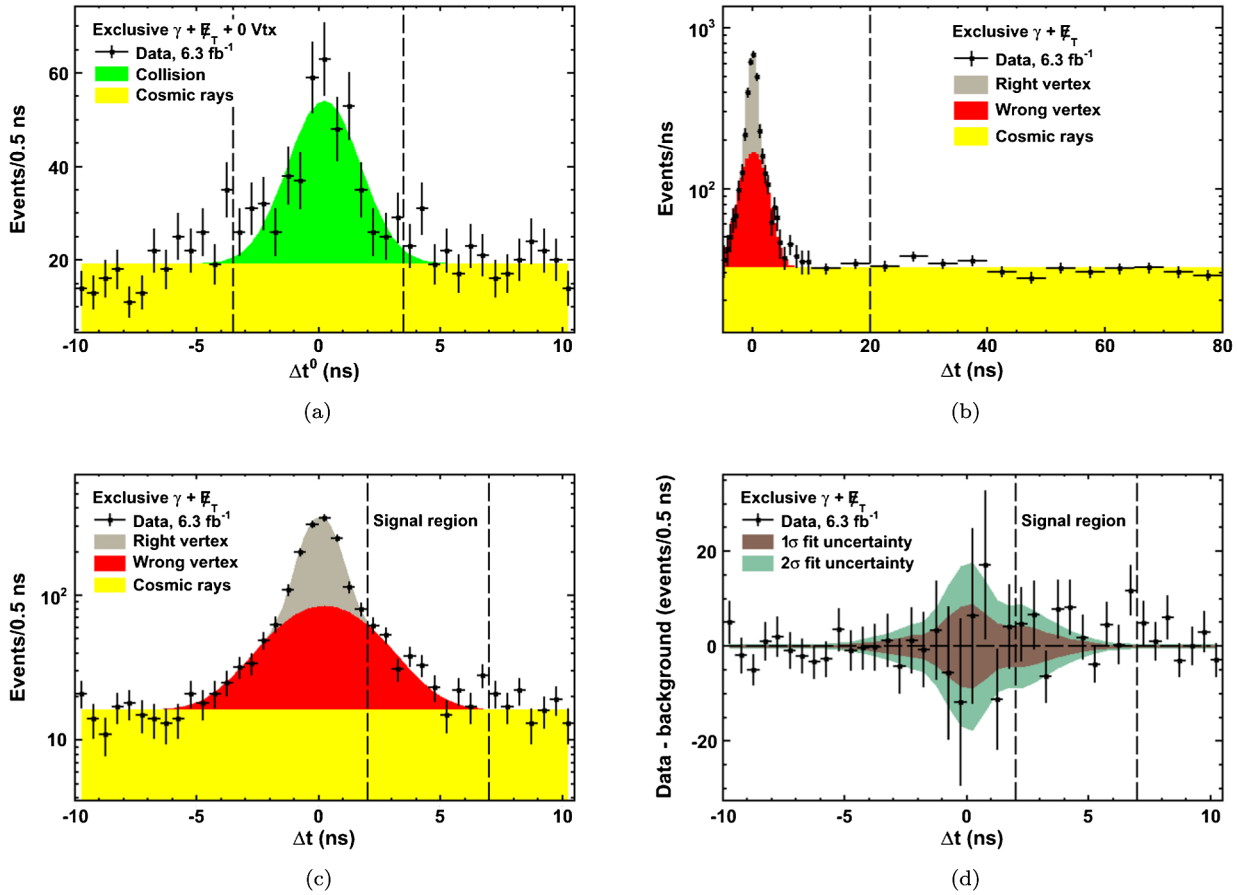

FIG. 2 (color online). (a) The Δt^0 timing distribution for $\gamma + \not{E}_T$ events with no vertex. The dashed lines demarcate the region $-3.5 < \Delta t^0 < 3.5$ ns, used to measure $\langle \Delta t^{\mathrm{W}} \rangle = \langle \Delta t^0 \rangle$. Note that the overflow and underflow data for cosmic-ray events beyond the timing regions shown in all figures have not been displayed. (b) The Δt timing distribution for $\gamma + \not{E}_T$ events with a vertex. The dashed line separates the region $20 < \Delta t < 80$ ns, which is used to estimate the rate of cosmic-ray events. (c) The Δt distribution, from $-10 < \Delta t < 10$ ns, with the dashed lines indicating the signal region. In all three cases, the shaded regions reflect the best-fit values determined from the sideband regions. (d) The background-subtracted data distribution with systematic uncertainties.

data-minus-background distribution is shown in Fig. 2(d). A total of 322 events are observed in the signal region. The probability for the SM background to yield the observed number of events or more (p value) is determined using simulated experiments that take into account the mean background expectation in the signal region, along with its systematic uncertainty. The resulting p value is 12%, consistent with standard model-only expectations.

In conclusion, motivated by the possible existence of an unobserved, heavy, long-lived, neutral particle, we present the first signature-based search for the production of events with the exclusive photon and missing transverse energy final state, where the photon detection time is delayed with respect to the time expected for a photon originated directly from the collision. We identify a number of kinematic properties and detector effects that can mimic the presence of a signal and use novel analysis techniques to minimize their impact on the results. We observe no evidence of delayed-photon production in this final state.

We thank the Fermilab staff and the technical staffs of the participating institutions for their vital contributions. This work was supported by the U.S. Department of Energy and National Science Foundation; the Italian Istituto Nazionale di Fisica Nucleare; the Ministry of Education, Culture, Sports, Science and Technology of Japan; the Natural Sciences and Engineering Research Council of Canada; the National Science Council of the Republic of China; the Swiss National Science Foundation; the A. P. Sloan Foundation; the Bundesministerium für Bildung und Forschung, Germany; the Korean World Class University Program, the National Research Foundation of Korea; the Science and Technology Facilities Council and the Royal Society, United Kingdom; the Russian Foundation for Basic Research; the Ministerio de Ciencia e Innovación, and Programa Consolider-Ingenio 2010, Spain; the Slovak R&D Agency; the Academy of Finland; the Australian Research Council (ARC); and the EU community Marie Curie Fellowship Contract No. 302103.

[1] S. L. Glashow, Nucl. Phys. **22**, 579 (1961); S. Weinberg, Phys. Rev. Lett. **19**, 1264 (1967); A. Salam, in *Elementary Particle Theory*, edited by N. Svartholm (Almqvist & Wiksell, Stockholm, 1968), p. 367.

[2] In the CDF II detector, a particle's direction is characterized by the azimuthal angle ϕ and the pseudorapidity $\eta = -\ln[\tan(\theta/2)]$, where the polar angle θ is measured with respect to the proton-beam direction. The transverse energy E_T is defined as $E\sin\theta$, where E is the energy in the electromagnetic and hadronic calorimeter towers associated with a cluster of energy deposition. The missing transverse energy $\vec{\not\!\!E}_T$ is defined as $\vec{\not\!\!E}_T = -\Sigma_i E_T^i \vec{n}_i$, where $\vec{n}_i$ is a unit vector in the transverse plane that points from the interaction vertex to the ith calorimeter tower. $\not\!\!E_T$ is the magnitude of $\vec{\not\!\!E}_T$. The cylindrical axis of the detector is denoted as the z coordinate and increases positively in the direction of the proton beam.

[3] D. A. Toback and P. Wagner, Phys. Rev. D **70**, 114032 (2004).

[4] J. D. Mason and D. Toback, Phys. Lett. B **702**, 377 (2011).

[5] M. Dine and W. Fischler, Phys. Lett. B **110**, 227 (1982); C. R. Nappi and B. A. Ovrut, Phys. Lett. B **113**, 175 (1982); L. Alvarez-Gaumé, M. Claudson, and M. B. Wise, Nucl. Phys. **B207**, 96 (1982); S. Dimopoulos and S. Raby, Nucl. Phys. **B219**, 479 (1983).

[6] A. Abulencia *et al.* (CDF Collaboration), Phys. Rev. Lett. **99**, 121801 (2007); T. Aaltonen *et al.* (CDF Collaboration), Phys. Rev. D **78**, 032015 (2008).

[7] A. Heister *et al.* (ALEPH Collaboration), Eur. Phys. J. C **25**, 339 (2002); M. Gataullin, S. Rosier, L. Xia, and H. Yang, AIP Conf. Proc. **903**, 217 (2007); G. Pásztor, Proc. Sci., HEP2005 (2005) 346; J. Abdallah *et al.* (DELPHI Collaboration), Eur. Phys. J. C **60**, 17 (2009); T. Aaltonen *et al.* (CDF Collaboration), Phys. Rev. Lett. **104**, 011801 (2010); V. M. Abazov *et al.* (D0 Collaboration), Phys. Rev. Lett. **105**, 221802 (2010); S. Chatrchyan *et al.* (CMS Collaboration), Phys. Rev. Lett. **106**, 211802 (2011); G. Aad *et al.* (ATLAS Collaboration), Phys. Rev. Lett. **106**, 121803 (2011); S. Chatrchyan *et al.* (CMS Collaboration), Phys. Lett. B **722**, 273 (2013); G. Aad *et al.* (ATLAS Collaboration), Phys. Rev. D **88**, 012001 (2013).

[8] J. Asaadi, Ph.D. thesis, Texas A&M University [Report No. FERMILAB-THESIS-2012-43]; A. Aurisano, Ph.D. thesis, Texas A&M University [Report No. FERMILAB-THESIS-2012-35].

[9] A. Abulencia *et al.* (CDF Collaboration), J. Phys. G **34**, 2457 (2007).

[10] A. Sill (CDF Collaboration), Nucl. Instrum. Methods Phys. Res., Sect. A **447**, 1 (2000).

[11] T. Affolder *et al.* (CDF Collaboration), Nucl. Instrum. Methods Phys. Res., Sect. A **526**, 249 (2004).

[12] M. Goncharov *et al.*, Nucl. Instrum. Methods Phys. Res., Sect. A **565**, 543 (2006).

[13] L. Balka *et al.*, Nucl. Instrum. Methods Phys. Res., Sect. A **267**, 272 (1988).

[14] T. Aaltonen *et al.* (CDF Collaboration), Phys. Rev. Lett. **101**, 181602 (2008).

[15] Since photons from collisions deposit greater quantities of energy in the hadronic calorimeter than do photon candidates from cosmic-ray events, we require the energy in the hadronic calorimeter element (HadE) immediately behind the electromagnetic calorimeter deposit associated with the photon to satisfy $\mathrm{HadE} > -0.30 + 0.008E_T^0$. Since photon candidates from cosmic-ray sources also deposit energy within the electromagnetic calorimeter differently than photons from collisions, we require the energy measured in the shower-maximum detector of the electromagnetic calorimeter to exceed 20% of the total energy

measured in the electromagnetic calorimeter [F. Abe *et al.* (CDF Collaboration), Phys. Rev. D **52**, 4784 (1995)].

[16] F. Abe *et al.* (CDF Collaboration), Phys. Rev. D **45**, 1448 (1992).

[17] T. Sjöstrand, P. Edén, C. Friberg, L. Lönnblad, G. Miu, S. Mrenna, and E. Norrbin, Comput. Phys. Commun. **135**, 238 (2001); T. Sjöstrand, S. Mrenna, and P. Skands, J. High Energy Phys. 05 (2006) 026.

[18] U. Baur, T. Han, and J. Ohnemus, Phys. Rev. D **57**, 2823 (1998).

[19] R. Brun, F. Bruyant, M. Maire, A. McPherson, and P. Zanarini, CERN Report No. CERN-DD/EE/84-1, 1987; we use the standard CDF simulation software as described in E. Gerchtein and M. Paulini, arXiv:physics/0306031 and add a parametrized timing simulation.

[20] Each electron is required to pass the standard electron requirements described in T. Aaltonen *et al.* (CDF Collaboration), Phys. Rev. D **77**, 112001 (2008), with the exception of the χ^2_{CES}, $|\Delta x|$ and $|\Delta z|$ requirements to make them more consistent with the photon identification requirements.

[21] W. Ashmanskas *et al.*, Nucl. Instrum. Methods Phys. Res., Sect. A **477**, 451 (2002); B. Ashmanskas *et al.*, Nucl. Instrum. Methods Phys. Res., Sect. A **518**, 532 (2004).